2024 IEEE/RSJ International Conference on Intelligent Robots and Systems (IROS)
October 14-18, 2024. Abu Dhabi, UAE

Strain-based Modeling of Rod-driven Soft Continuum Robots with Co-located Embedded Sensors

Peiyi Wang*, Daniel Feliu-Talegon*, Sheng Guo, Federico Renda and Cecilia Laschi

Abstract— **Rod-driven soft robots (RDSR) with a well-balanced performance in terms of perception, precision, and intelligence have a great potential for application. Mathematical description and predicted sensing of deformable soft bodies are crucial to achieve controllable and intelligent behaviors of these robots. In this work, we propose a kinetostatic model for RDSR embedded with co-located sensors based on the Geometric Variable Strain (GVS) approach where local deformations, actuation lengths and external interactions are included. This approach allows us to estimate the shape of RDSR and predict the strain variation of soft bodies under internal and external interactions. Simulations and experimental results show that tip position errors are not greater than 1.8% with respect to the whole body length under different loads (0, 100, 200, 300 gf). The maximum error of predicted sensor length change is up to 2 mm and its percentage relative to the actual length does not exceed 4%. The results demonstrate the accuracy and effectiveness of the proposed model.**

I. INTRODUCTION

Continuum robots have emerged as a promising paradigm in the field of soft robotics, offering unprecedented flexibility and adaptability for a wide range of applications [1], [2]. Among these, the rod-driven soft robot (RDSR) stands out as a multifunctional system capable of active push-pull actuation, complex movements, and adaptable shape changes [3]. Different from cables and fluid channels [4], [5], flexible rods provide precise and stable length feedback inside the soft body. Such exact information is hard to find in soft robotics because their overall shape varies with any internal actuation and external disturbances [1], [6]. Sensing methods involving purposive sensors such as joint encoders and force/torque sensors in rigid-link robots are also feasible in RDSR based on deterministic structures, co-located sensors and accurate models. A mathematical description and direct perception of deformable soft bodies are crucial to achieve controllable and intelligent performance of RDSR [6], [7].

This work funded in part by the National Natural Science Foundation of China (Grant no. 52275004) and Beijing Natural Science Foundation (Grant no. 3242012), in part by REBOT (Rethinking underwater robot manipulation), Ministry of Education, Singapore, Moe-t2eP50221-0010. This work was also supported by the US Office of Naval Research Global under Grant N62909- 21-1-2033 and in part by Khalifa University under Awards No. RIG-2023-048, RC1-2018- KUCARS.

*These two authors contribute equally to this work

Peiyi Wang and Cecilia Laschi are with Department of Mechanical Engineering, National University of Singapore, Singapore, Singapore(email: peiyi.wang@nus.edu.sg, mpeclc@nus.edu.sg)

Sheng Guo is with Robotics Research Center, Beijing Jiaotong University, Beijing, China(e-mail: shguo@bjtu.edu.cn)

Daniel Feliu-Talegon and Federico Renda are with department of Mechanical and Nuclear Engineering, Khalifa University of Science and Technology Abu Dhabi, UAE (email: daniel.talegon@ku.ac.ae, federico.renda@ku.ac.ae)

Pure kinematic models reveal mapping relationships between configuration and actuator space and between configuration and task space [8]. Co-located sensors strategically aligned with bending segments performed well in estimating shape parameters, enabling proprioception and disturbance observation of soft robotic arms [9], [10], [11]. Nevertheless, this method overlooks the impact of external factors such as gravity, friction, and environmental interactions, despite the real-time local strain capture capability of co-located sensors. To accurately predict the shape and local strains of soft robots, kinematic parameters such as actuation variables, and physical parameters such as elasticity, internal and external interactions must be included in the mathematical model [6], [7]. 3D continuum solid mechanics such as finite element method (FEM) and Cosserat rod model allows all degrees of freedom (DOFs) to be described for all topologies required for soft robots. The FEM approach discretizes the soft body into a large number of elements. The convergent solutions involves extensive computational processes, depending on element number, mesh quality and boundary constraints. Consequently, model order reduction and substantial simplification are required to maintain good accuracy and real-time computation of dynamics and robot control [12]. The Cosserat rod theory is the most used in continuum robot such as concentric tube continuum robots [13], tendon-driven continuum robots (TACRs) [14], and multibackbone continum robots [15], [16] for modelling the statics and dynamics of such systems [17]. A shooting-based method was mostly proposed to solve the boundary value problem of the Cosserat rod equation. However, this theory currently does not specifically model continuum robots with soft bodies and flexible rod actuation [3], and the root-finding process of convergent solutions is time-consuming [14]. Recently, a novel strain-based modelling method, named the Geometric Variable Strain (GVS) apporach [18], [19], was developed from Cosserat model by discretizing the continous soft body into a finite set of strain basis functions. This GVS approach is a generalization of other rigid and soft robots' model, such as constant curvature for continuum robots [8] and joint-based modelling of rigid robots [20]. The GVS-based model proved to be excellent in all cases, both in terms of accuracy and complexity for tendon-driven, fluid-driven and concentric tube soft continuum robots [18], [21], [22]. Benefiting from the variable basis functions of the discrete model, the GVS approach can explicitly develop the geometric Jacobian and actuation matrix of soft robots. On this basis, static and dynamic model-based control in real time are feasible for this field [23], [24]. Besides, by

combining with sensor readings, the researcher demonstrated the effectiveness of GVS approach in perceiving robot's shape and external tip forces [25]. Overall, this approach still needs to be explored and researched in many aspects in the field of soft robotics.

In this work, we explore the possibility of applying the discrete model based on the GVS approach to RDSR. The model is specifically built for a hybrid soft structure with a silicon-based body and flexible rod. By inputting rod lengths and external loads, we can estimate the shape of RDSR and predict the local stain in selected segments.

The manuscript is organized as follows. Section II descries the fundamental formulas of GVS approach. Section III presents the RDSR systems. Section IV shows simulations and experimental results to demonstrate the accuracy of estimated shape and predicted strain. Finally, the manuscripts ends with conclusions and discussions in Section V.

II. GEOMETRIC VARIABLE STRAIN MODEL

In this section, we outline the fundamental elements of GVS model and provide the static equilibrium equations applicable to the robot under investigation. For a detailed description of the GVS approach for static modelling, the reader is referred to [18].

A. Robot Kinematics

Our robot consists of a hybrid kinematic chain of rigid and soft parts which can represented by Cosserat rods. The configuration of a slender soft body i can be modeled as a continuous stack of rigid cross-sections parameterized by a curvilinear abscissa $X_i \in [0, L_i]$, where L_i is the length of the rod i (Fig. 1). The homogeneous transformation matrix representing a coordinate frame attached to these cross-sections is defined as the directed spatial curve $\boldsymbol{g_i}(\bullet) : X_i \rightarrow \boldsymbol{g}_i(X_i) \in SE(3)$:

$$\boldsymbol{g}_i(X) = \begin{bmatrix} \boldsymbol{R}_i & \boldsymbol{r}_i \\ \boldsymbol{0} & 1 \end{bmatrix}, \tag{1}$$

where $\boldsymbol{r}_i(X) \in \mathbb{R}^3$ is the position of the local frame, while $\boldsymbol{R}_i(X) \in SO(3)$ provides the orientation of the local frame relative to the spatial frame. Strain $\boldsymbol{\xi}_i$ and velocity $\boldsymbol{\eta}_i$ twists of the body are defined by the partial derivative of Equation (1) with respect to space $(\cdot)'$ and time $\dot{(\cdot)}$:

$$\boldsymbol{g}_i'(X_i) = \boldsymbol{g}_i\hat{\boldsymbol{\xi}}_i, \qquad \dot{\boldsymbol{g}}_i(X_i) = \boldsymbol{g}_i\hat{\boldsymbol{\eta}}_i, \tag{2}$$

where $\hat{(\bullet)}$ indicates the isomorphism between $\mathbb{R}^6$ and $se(3)$. Space integration of the left part of equation (2) provides:

$$\boldsymbol{g}_i(X_i) = \exp\left(\widehat{\boldsymbol{\Omega}}_i(X_i)\right), \tag{3}$$

where $\boldsymbol{\Omega}_i(X)$ is the Magnus expansion of $\boldsymbol{\xi}_i(X_i)$. The exponential map in SE(3) and the Lie algebra associated with a Lie group used in this section can be found in [26]. The soft links are divided into smaller intervals of lengths h and $\boldsymbol{g}_i(X_i)$ is computed recursively through these intervals

$$\boldsymbol{g}_i(X_i + h) = \boldsymbol{g}_i(X_i)\exp\left(\widehat{\boldsymbol{\Omega}}_i(h)\right), \tag{4}$$

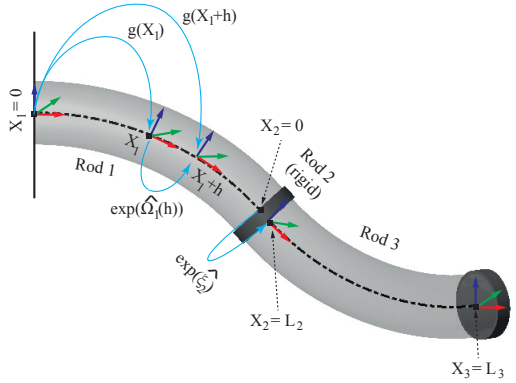

Fig. 1: Schematic of the GVS kinematics approach illustrating with the recursive formulation of the kinematic of the robot $g_i(X_i)$.

For the case of a rigid link i the configuration is divided in two: the initial configuration $X_i = 0$ and, the final $X_i = L_i$:

$$\boldsymbol{g}_i(L_i) = \boldsymbol{g}_i(0)\exp\left(\widehat{\boldsymbol{\xi}}_i\right), \tag{5}$$

where $\widehat{\boldsymbol{\xi}}_i$ for rigid links is constant.

The relation between screw strain and velocity is established through the equality of the mixed partial derivatives in space and time:

$$\boldsymbol{\eta}_i' = \dot{\boldsymbol{\xi}}_i - \mathrm{ad}_{\boldsymbol{\xi}_i}\boldsymbol{\eta}_i \tag{6}$$

where $\mathrm{ad}_{(\bullet)} \in \mathbb{R}^{6\times6}$ is the adjoint operator of $se(3)$. By virtue of the identity $(\mathrm{Ad}_{\boldsymbol{g}_i})' = \mathrm{Ad}_{\boldsymbol{g}_i}\mathrm{ad}_{\boldsymbol{\xi}_i}$ and the Leibniz rule for the derivative of a product, it can be verified that the analytic solution of (6) is given by:

$$\boldsymbol{\eta}_i(X_i) = \mathrm{Ad}_{\boldsymbol{g}_i^{-1}}\int_0^X \mathrm{Ad}_{\boldsymbol{g}_i}\dot{\boldsymbol{\xi}}_i ds \tag{7}$$

where $\mathrm{Ad}_{\boldsymbol{g}_i}$ is the adjoint representation of $\boldsymbol{g}_i$.

The strain field $\boldsymbol{\xi}_i$ can be discretized by choosing a specific set of vector functions to serve as a finite basis for the field. This can be represented as:

$$\boldsymbol{\xi}_i(X_i) = \boldsymbol{\Phi}_{\xi_i}(X_i)\boldsymbol{q} + \boldsymbol{\xi}_i^*(X_i) \tag{8}$$

where $\boldsymbol{\Phi}_{\xi_i}(X_i) \in \mathbb{R}^{6\times n}$ is the matrix function whose columns form the basis for the strain field, $\boldsymbol{q} \in \mathbb{R}^n$, n being the $DoFs$, is the vector of generalized coordinates for the chosen basis function. Equation (8) can be substituted into equation (6), eventually leading to the definition of geometric Jacobian and its derivative:

$$\boldsymbol{\eta}_i(X_i) = \mathrm{Ad}^{-1}_{\boldsymbol{g}_i(X_i)}\int_0^{X_i} \mathrm{Ad}_{\boldsymbol{g}_i}\boldsymbol{\Phi}_{\xi_i} ds\dot{\boldsymbol{q}} = \boldsymbol{J}_i(\boldsymbol{q}, X_i)\dot{\boldsymbol{q}} \tag{9}$$

Although (3) and (9) are analytical expressions, for a general variable strain case, they cannot be computed explicitly. The GVS approach employs a finite set of strain bases to discretize in intervals the continuous strain field. In this work, we use the fourth order Zanna collocation approach with two-stage Gauss quadrature as detailed in [27].

B. Actuation load of the robot

Rod-driven soft robot is a versatile system capable of active push-pull actuation. We consider our system as a Cosserat rod internally actuated by several rods similar to cables and fluidic actuation [18]. The actuation load in the body i is obtained by computing the force and moment exerted by the internal rods on the mid-line of the rod

$$\boldsymbol{\mathcal{F}}_{a_i}(X_i) = \sum_{k=1}^{n_{a_i}} \begin{bmatrix} \tilde{\boldsymbol{d}}_{ik}\boldsymbol{t}_{ik} \\ \boldsymbol{t}_{ik} \end{bmatrix} u_{ik} = \boldsymbol{\Phi}_{a_i}(\boldsymbol{q}, X)\boldsymbol{u}_i, \quad (10)$$

where $\boldsymbol{\Phi}_{a_i}(\boldsymbol{q}, X) \in \mathbb{R}^{6\times n_a}$ is the actuation basis, n_a is the number of actuators, $\boldsymbol{d}_{ik}(X) \in \mathbb{R}^3$ is the distance from the mid-line to actuator k, $\boldsymbol{t}_{ik}(X) \in \mathbb{R}^3$ is the unit vector tangent to the actuator's path, $\boldsymbol{u}_i$ is the magnitude of the actuation force and $\tilde{\bullet}$ is the skew-symmetric matrix representation of $so(3)$.

C. Elasticity Model

In order to complete the static equilibrium model for our robot the internal elastic has to be developed. We propose to use a Hook-like linear elastic law to describe the rod elasticity:

$$\boldsymbol{\mathcal{F}}_{e_i}(X_i) = \boldsymbol{\Sigma}_i(X_i)(\boldsymbol{\xi}_i(X_i) - \boldsymbol{\xi}^*(X_i)), \quad (11)$$

where $\boldsymbol{\Sigma}_i(X_i) = \text{diag}(G_iJ_{x_i},\ E_iJ_{y_i},\ E_iJ_{z_i},\ E_iA_i,\ G_iA_i,\ G_iA_i) \in \mathbb{R}^{6\times6}$ is the screw elasticity matrix, E_i being the Young modulus and G_i the shear modulus.

D. Static equilibrium of the robot

The discrete model that represents the static equilibrium of our system can be obtained by projecting the equilibrium equations by means of D'Alembert Principle:

$$\boldsymbol{K}(\boldsymbol{q}) = \boldsymbol{B}(\boldsymbol{q})\,\boldsymbol{u} + \boldsymbol{Q}_e(\boldsymbol{q}), \quad (12)$$

where $\boldsymbol{K}(\boldsymbol{q})$ is the generalized internal elastic force, $\boldsymbol{Q}_e(\boldsymbol{q})$ is the vector of generalized external forces, $\boldsymbol{B}(\boldsymbol{q})$ is the generalized actuation matrix, and $\boldsymbol{u}$ is the vector of applied actuation forces.

$$\boldsymbol{K}(\boldsymbol{q}) = ||_{i=1}^{N}\left(\int_0^{L_i} \boldsymbol{\Phi}_{\xi_i}^T \boldsymbol{\Sigma}_i \boldsymbol{\Phi}_{\xi_i} dX\right) \quad (13)$$

$$\boldsymbol{B}(\boldsymbol{q}) = diag_{i=1}^{N}\left(\int_0^{L_i} \boldsymbol{\Phi}_{\xi_i}^T \boldsymbol{\Phi}_{a_i} dX\right) \quad (14)$$

$$\boldsymbol{Q}_e(\boldsymbol{q}) = \sum_{i=1}^{N}\int_0^{L_i} \boldsymbol{J}_i^T \overline{\boldsymbol{\mathcal{F}}}_{e_i} dX \quad (15)$$

where $||$ is the vector concatenation operator, N is the total number of links and $\overline{\boldsymbol{\mathcal{F}}}_{e_i}$ are the external forces applied to the system. Similar to $\boldsymbol{g}_i$, the geometric Jacobian $\boldsymbol{J}_i$ is recursively computed using the approximated form of Magnus expansion. For more comprehensive details, readers may refer to [21], where the static and dynamic analysis of soft-rigid hybrid robots with multidimensional rigid joints is discussed. This reference also includes the derivation of the key equations described in the proposed model.

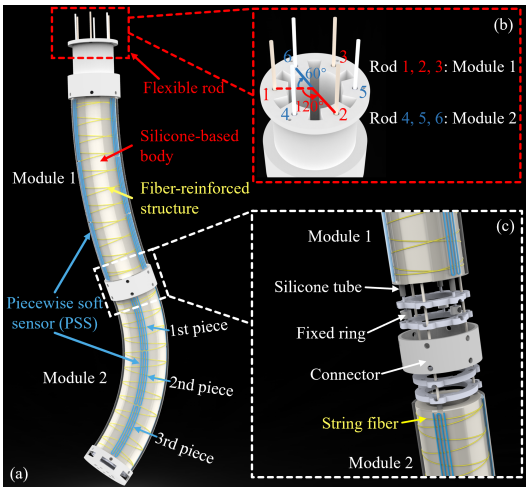

Fig. 2: The description of robot system. (a) The whole system design. (b) Flexible rod distribution of each module. (c) Detailed structure of the connected location of two modules.

E. Length kinematic equation

The kinematic equation relating the change in length of each actuator (y_k) with the state of the manipulator is given by [27].

$$y_k = \int_0^L \boldsymbol{\Phi}_{a_k}^T \boldsymbol{\Phi}_{\boldsymbol{\xi}_i} dX + \int_0^L (\boldsymbol{\Phi}_{ak} - \boldsymbol{\Phi}_{ak}^*)^T \left(\boldsymbol{\xi}^* - \begin{bmatrix} \boldsymbol{0} \\ \boldsymbol{d}_k' \end{bmatrix}\right) dX \quad (16)$$

The above equation can be represented in matrix form by gathering the change in length for each actuator in a single vector:

$$\boldsymbol{y_a} = \boldsymbol{B}(\boldsymbol{q})^T\boldsymbol{q} + \boldsymbol{z_a}(\boldsymbol{q}) \quad (17)$$

The above equation also serves to establish a relationship between the length of the sensors and the deformation of the soft robot in the segments where these sensors are positioned. Therefore, the integration of equation (16) is computed only within the regions corresponding to the sensor locations.

III. SOFT CONTINUUM ROBOT SYSTEM

A two-module RDSR was designed and fabricated as shown in Fig. 2a, which is a modification of our previous design [3] with piecewise soft sensors (PSS) embedded on the surface. A detailed description of the actuation, collection, and control systems can be found in previous publication [3].

Each module consists of a silicone-based body, three PSS, fiber-reinforced structure, constraint disks, three silicone tubes hosting the corresponding flexible rod each of NiTi, and three lock rings. The flexible rods of each module are evenly distributed along the circumferential direction Fig. 2b. The silicone-based body has an initial length of 160 mm. It is located between two constraint disks and reinforced by a fiber structure that reduces radial deformation and achieves larger bending capabilities when pushing and pulling the flexible rods. One-module RDSR realizes elongation, shortening, and bending through coordinated control

TABLE I: Evaluation of the formula developed for computing the equivalent elasticity matrix of our robot through testing.

Force (gf)	X_m (mm)	Z_m (mm)	X_e (mm)	Z_e (mm)	$Error$ (mm)
0	162	−29	158	−25	5.7
100	149	−63	148	−58	5.1
200	133	−87	135	−84	3.6
400	106	−111	112	−112	6.1

of three push-pull rods. Multi-module RDSRs are assembled in series, via the 3D printed connector (Fig. 2c). The flexible rod of module 2 passes through the soft body of module 1.

Each PSS, consisting of three pieces (1st, 2nd, 3rd piece), is embedded on the surface of the silicone-based body and string fiber. To accurate capture of local strain, the PSS with a thickness of 1 mm is aligned to the corresponding rod. The initial length of each unstretched PSS is 130 mm, respectively. Each piece has the same length, about 42 mm. The strain in all sensors remains the same when the silicone substrate is deformed. During the fabrication process, the silicone-based body is compressed to maintain the same length as the PSS. In this way, after the soft body returns to its original length, the PSS is stretched and the bidirectional strain changes can be captured.

IV. EXPERIMENT VERIFICATION

A. Screw elasticity matrix of our robot

The system proposed here consists of a silicone body with NiTi Rod inside it. Because of the symmetrical arrangement of the rods, the center of elasticity coincides with the geometrical center. However, the stiffness contributed by the elastic rods needs to be incorporated. To derive the equivalent elasticity matrix $\mathbf{\Sigma}_i(X_i)$ of our system, the following formula has been devised.

$$\mathbf{\Sigma}_i(X_i) = \mathbf{\Sigma}^1 + \sum_{k=1}^{n_{a_i}} \left(Ad^*_{\boldsymbol{g}^k} \mathbf{\Sigma}^3 Ad^{-1}_{\boldsymbol{g}^k} - Ad^*_{\boldsymbol{g}^k} \mathbf{\Sigma}^2 Ad^{-1}_{\boldsymbol{g}^k} \right), \tag{18}$$

where $\boldsymbol{g}^k$ represents the transformation matrix from the center of rod k to the centerline of the soft robot, $\mathbf{\Sigma}^1$ is the elasticity matrix of the entire silicone body, while $\mathbf{\Sigma}^2$ represents the elasticity matrix treating the rods as silicone. Additionally, $\mathbf{\Sigma}^3$ denotes the elasticity matrix for the rods alone. When incorporating the stiffness of the rods, the terms that generates forces in the elasticity matrix are excluded in the calculation since they are already incorporated in the actuation load (10). Then, $\mathbf{\Sigma}^1 = \text{diag}(G^b J^b_x,\ E^b J^b_y,\ E^b J^b_z,\ E^b A^b,\ G^b A^b,\ G^b A^b)$, $\mathbf{\Sigma}^2_i = \text{diag}(G^b J^r_x,\ E^b J^r_y,\ E^b J^r_z,\ 0,\ 0,\ 0)$ and $\mathbf{\Sigma}^3_i = \text{diag}(G^r J^r_x,\ E^r J^r_y,\ E^r J^r_z,\ 0,\ 0,\ 0)$. Here, the superscripts r and b denote the properties for the rods and the soft body, respectively. We test the equivalent elasticity matrix using one of the soft link of the robot, housing three rods inside it, and without clamping them at the base. The results show a maximum error of 6.1 mm which is approximately 4% the length of the rod (Table I).

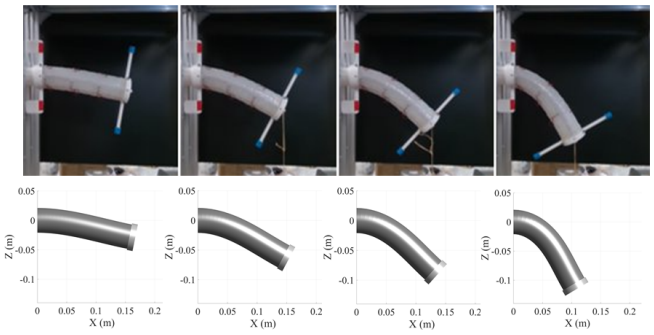

Fig. 3: Assessing the accuracy of formula (18) by comparing simulations with experimental results.

TABLE II: Shape and material parameters of RDSR

NiTi Rod	Young's Modulus (GPa)	10
	Radius (mm)	0.65
	Position radius (mm)	16
Silicone body	Young's Modulus (KPa)	110
	Initial length (mm)	160
	Inner radius (mm)	12.5
	Outer radius (mm)	21
Fiber position radius (mm)		18
Sensors position radius (mm)		21
Length of connector (mm)		10

B. Forward solutions

The complete kinetostatic model of our robot is described by equation (12) and (17). The solving process is similar to the forward statics of conventional robots, where rods length $\boldsymbol{y}_a$ and external forces, $\overline{\boldsymbol{\mathcal{F}}}_{e_i}$, can be used to calculate the shape of the RDSR, $\boldsymbol{q}$, and the actuation loads $\boldsymbol{u}$. For these inputs and outputs, a system of $n + n_a$ nonlinear equations and $n + n_a$ unknowns can be solved using a root finding algorithm. We implement the trust-region-dogleg algorithm through the MATLAB function *fsolve* to solve the system. Once, the shape of the RDSR is computed, the estimated length of the sensors can be obtained by computing equation (17) but considering the position of the sensors. The simulated shape of the RDSR is solved under different tip forces and rod lengths. The shape and material parameters of RDSR used in model are shown in Table II. We validate the proposed model using a constant Legendre polynomial basis for elongation and third-order Legendre polynomial basis for the two bending direction (y, z) for each soft link, resulting in a total of 18 DOFs.

We can simulate different robot configurations under variable rod lengths and external loads. The soft body is shortened when all flexible rods are pulled. Inversely, the robot is elongated. More complex configurations, such as "S" and "C" shape bending (Fig. 4), can be achieved by coordinating rod lengths. For the 'S' and 'C' shapes presented, the lengths of rod 1 to 6 are [150, 160, 180, 310, 310, 340] mm and [160, 145, 160, 290, 290, 320] mm, respectively.

C. Data collection process

Initially, we randomly generated 500 experimental configurations of RDSR. The robot can be defined by arc

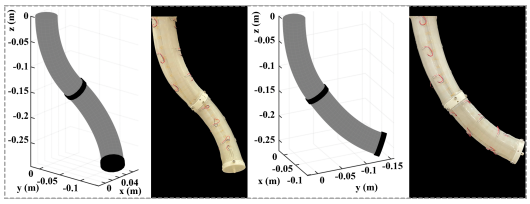

Fig. 4: Theoretical simulations and experimental configurations of 'S' and 'C' shape bending of a two-module RDSR.

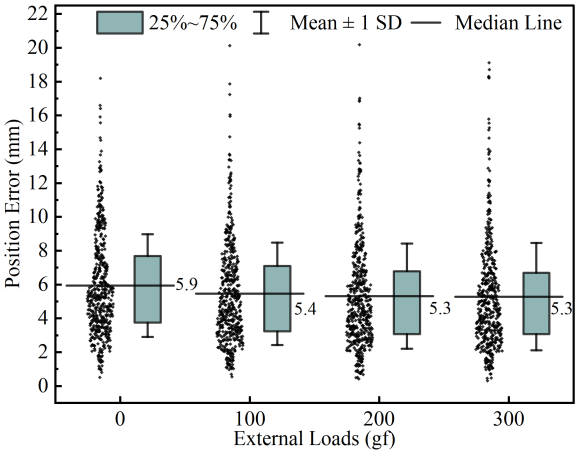

Fig. 5: Tip position error distribution and box plot of RDSR under different external loads (0, 100, 200, 300 gf).

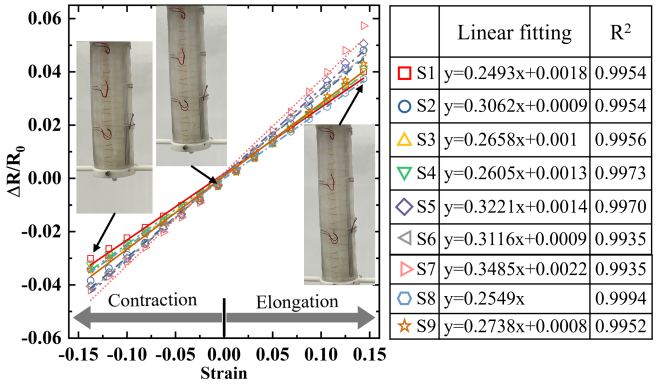

	Linear fitting	R^2
S1	y=0.2493x+0.0018	0.9954
S2	y=0.3062x+0.0009	0.9954
S3	y=0.2658x+0.001	0.9956
S4	y=0.2605x+0.0013	0.9973
S5	y=0.3221x+0.0014	0.9970
S6	y=0.3116x+0.0009	0.9935
S7	y=0.3485x+0.0022	0.9935
S8	y=0.2549x	0.9994
S9	y=0.2738x+0.0008	0.9952

Fig. 6: Calibration process and fitting results of one-module RDSR with PSS.

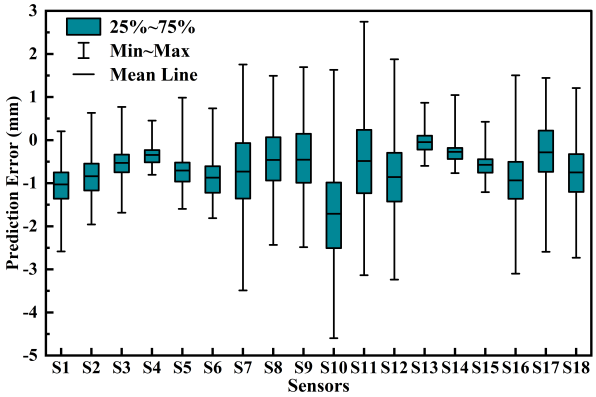

Fig. 7: The prediction errors for all sensor length changes under 300 gf external load.

parameters consisting of arc length Lc, bending angle β and the angle of bending plane ϕ. Lc ranges from 155 to 165 mm. ϕ ranges from 0 to 2π. β ranges from 0 to 40°. Then, the RDSR was actuated without and with different external loads (100, 200, 300 gram-force(gf)). Tip position was recorded by a RGB-D camera (RealSense D435), and the recorded data was used as the ground truth. The sensor voltage was acquired by DAQ (NI USB-6218).

D. Tip position accuracy

For each configuration and load condition, the established model obtains the entire shape and every position along the body. The error e is calculated from estimated position $\mathbf{p}_{model}$ and recorded ground truth $\mathbf{p}_{actual}$ from RGB-D camera. $e = ||\mathbf{p}_{model} - \mathbf{p}_{actual}||$. These errors under different external loads (0, 100, 200, 300 gf) are shown in Fig. 5. The errors on average are less than 6 mm with respect to different loads. The corresponding error percentages are not greater than 1.8% relative to the body length (330 mm). Judging from the error distribution, most of them locate around 5 mm, ranging from 3 to 8 mm. The model accurately describes the deformation of the RDSR under actuation and external loads.

E. Predicted sensor strain

There are 18 pieces of sensor in the whole system. For convenience, we name these sensors S1 to S18 in order from the 1st to 3rd piece of Rod 1 to 6 as shown in Fig. 2.

The calibration process and fitting results of sensors are shown in Fig. 6. The robot shortens from its original length and then stretches from its shortest state to its longest state. All rods are simultaneously pulled or pushed to achieve extensible movement. Since the rod length is exactly known, all sensor lengths are obtained by dividing the rod length by three. At the same time, we record the change of sensor resistance. Finally, the calibration results between the resistance change rate and the sensor strain are fitted. Results show that the sensor has good linearity with a goodness of fit close to 1. Once the resistance is obtained, the sensor length or strain can be estimated based on these relationships.

By inputting the start and end positions of each sensor, the model can predict local strains in real time. As measured from the real prototype, the start and end positions of the sensor aligned with rod 1 in module 1 are (3, 55, 107) mm and (53, 105, 157) mm, respectively. Then, the prediction error for sensor length changes is calculated, $e_{sensor} = \Delta l_{prediction} - \Delta l_{actual}$. $\Delta l_{prediction}$ is model estimation. Δl_{actual} is obtained from sensor recordings and calibrations.

Taking the experimental configuration under 300 gf external loads as an example, the error distribution of all sensor length changes is presented in Fig. 7. Most prediction errors are no more than 2.5 mm, with the average being within 2 mm, but some sensors have larger error ranges, especially the S10, S11 and S12.

To better measure the performance of predictions, the root-

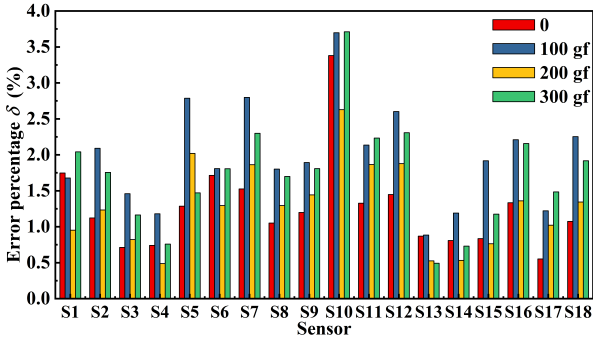

Fig. 8: The error percentage of predicted sensor length under 0, 100, 200, 300 gf loads.

mean-square error (RMSE) and its percentage are calculated:

$$\delta_{sensor} = \sqrt{\frac{1}{n}\sum_{i=1}^{n}\left(\frac{\Delta l_{prediction} - \Delta l_{actual}}{l_{actual}}\right)^2} \tag{19}$$

The maximum RMSE can be up to 2 mm and its percentage (shown in Fig. 8) relative to the actual sensor length does not exceed 4 %, which occurs in the S10. The prediction error of other sensors under different external loads are no more than 3% of its actual length. The variable-strain model can accurately predict the sensor strain.

V. CONCLUSION

In this paper, a discrete Cosserat static model for RDSR based on GVS approach was developed, which includes local deformation of body, actuation length of rods and environmental interactions. We specifically built the screw elasticity matrix for a hybrid soft structure consisting of a silicone-based body and a flexible rod. On this basis, the model can estimate the entire robot shape and predict local strain changes in selected segments. The experimental results demonstrate the accuracy and effectiveness of the proposed model, with errors in estimated position and local sensor length not exceeding 1.8% and 4%, respectively. In future work, we will explore the application of the discrete static model in force sensing and intelligent motion control.

REFERENCES

[1] C. Laschi, B. Mazzolai, and M. Cianchetti, "Soft robotics: Technologies and systems pushing the boundaries of robot abilities," *Science robotics*, vol. 1, no. 1, p. eaah3690, 2016.

[2] M. Russo, S. M. H. Sadati, X. Dong, A. Mohammad, I. D. Walker, C. Bergeles, K. Xu, and D. A. Axinte, "Continuum robots: An overview," *Advanced Intelligent Systems*, vol. 5, no. 5, p. 2200367, 2023.

[3] P. Wang, Z. Tang, W. Xin, Z. Xie, S. Guo, and C. Laschi, "Design and experimental characterization of a push-pull flexible rod-driven soft-bodied robot," *IEEE Robotics and Automation Letters*, vol. 7, no. 4, pp. 8933–8940, 2022.

[4] M. Cianchetti, T. Ranzani, G. Gerboni, I. De Falco, C. Laschi, and A. Menciassi, "Stiff-flop surgical manipulator: Mechanical design and experimental characterization of the single module," in *2013 IEEE/RSJ international conference on intelligent robots and systems*. IEEE, 2013, pp. 3576–3581.

[5] D. Alatorre, D. Axinte, and A. Rabani, "Continuum robot proprioception: the ionic liquid approach," *IEEE Transactions on Robotics*, vol. 38, no. 1, pp. 526–535, 2021.

[6] G. Mengaldo, F. Renda, S. L. Brunton, M. Bächer, M. Calisti, C. Duriez, G. S. Chirikjian, and C. Laschi, "A concise guide to modelling the physics of embodied intelligence in soft robotics," *Nature Reviews Physics*, vol. 4, no. 9, pp. 595–610, 2022.

[7] C. Armanini, F. Boyer, A. T. Mathew, C. Duriez, and F. Renda, "Soft robots modeling: A structured overview," *IEEE Transactions on Robotics*, vol. 39, no. 3, pp. 1728–1748, 2023.

[8] R. J. Webster III and B. A. Jones, "Design and kinematic modeling of constant curvature continuum robots: A review," *The International Journal of Robotics Research*, vol. 29, no. 13, pp. 1661–1683, 2010.

[9] R. L. Truby, C. Della Santina, and D. Rus, "Distributed proprioception of 3d configuration in soft, sensorized robots via deep learning," *IEEE Robotics and Automation Letters*, vol. 5, no. 2, pp. 3299–3306, 2020.

[10] C. Della Santina, R. L. Truby, and D. Rus, "Data–driven disturbance observers for estimating external forces on soft robots," *IEEE Robotics and automation letters*, vol. 5, no. 4, pp. 5717–5724, 2020.

[11] Z. Xie, F. Yuan, Z. Liu, Z. Sun, E. M. Knubben, and L. Wen, "A proprioceptive soft tentacle gripper based on crosswise stretchable sensors," *IEEE/ASME Transactions on Mechatronics*, vol. 25, no. 4, pp. 1841–1850, 2020.

[12] O. Goury and C. Duriez, "Fast, generic, and reliable control and simulation of soft robots using model order reduction," *IEEE Transactions on Robotics*, vol. 34, no. 6, pp. 1565–1576, 2018.

[13] J. Ha, G. Fagogenis, and P. E. Dupont, "Modeling tube clearance and bounding the effect of friction in concentric tube robot kinematics," *IEEE Transactions on Robotics*, vol. 35, no. 2, pp. 353–370, 2019.

[14] J. Till, V. Aloi, and C. Rucker, "Real-time dynamics of soft and continuum robots based on cosserat rod models," *The International Journal of Robotics Research*, vol. 38, no. 6, pp. 723–746, 2019.

[15] A. L. Orekhov, V. A. Aloi, and D. C. Rucker, "Modeling parallel continuum robots with general intermediate constraints," in *2017 IEEE International Conference on Robotics and Automation (ICRA)*, 2017, pp. 6142–6149.

[16] P. Wang, S. Guo, X. Wang, and Y. Wu, "Design and analysis of a novel variable stiffness continuum robot with built-in winding-styled ropes," *IEEE Robotics and Automation Letters*, vol. 7, no. 3, pp. 6375–6382, 2022.

[17] M. Tummers, V. Lebastard, F. Boyer, J. Troccaz, B. Rosa, and M. T. Chikhaoui, "Cosserat rod modeling of continuum robots from newtonian and lagrangian perspectives," *IEEE Transactions on Robotics*, vol. 39, no. 3, pp. 2360–2378, 2023.

[18] F. Renda, C. Armanini, V. Lebastard, F. Candelier, and F. Boyer, "A geometric variable-strain approach for static modeling of soft manipulators with tendon and fluidic actuation," *IEEE Robotics and Automation Letters*, vol. 5, no. 3, pp. 4006–4013, 2020.

[19] F. Boyer, V. Lebastard, F. Candelier, and F. Renda, "Dynamics of continuum and soft robots: A strain parameterization based approach," *IEEE Transactions on Robotics*, vol. 37, no. 3, pp. 847–863, 2020.

[20] K. M. Lynch and F. C. Park, *Modern robotics: Mechanics, Planning, and Control*. Cambridge University Press, 2017.

[21] A. T. Mathew, I. B. Hmida, C. Armanini, F. Boyer, and F. Renda, "Sorosim: A matlab toolbox for hybrid rigid–soft robots based on the geometric variable-strain approach," *IEEE Robotics and Automation Magazine*, vol. 30, no. 3, pp. 106–122, 2022.

[22] F. Renda, C. Messer, C. Rucker, and F. Boyer, "A sliding-rod variable-strain model for concentric tube robots," *IEEE Robotics and Automation Letters*, vol. 6, no. 2, pp. 3451–3458, 2021.

[23] H. Li, L. Xun, G. Zheng, and F. Renda, "Discrete cosserat static model-based control of soft manipulator," *IEEE Robotics and Automation Letters*, vol. 8, no. 3, pp. 1739–1746, 2023.

[24] F. Renda, A. Mathew, and D. F. Talegon, "Dynamics and control of soft robots with implicit strain parametrization," *IEEE Robotics and Automation Letters*, 2024.

[25] A. Y. Alkayas, D. Feliu-Talegon, A. T. Mathew, C. Rucker, and F. Renda, "Shape and tip force estimation of concentric tube robots based on actuation readings alone," in *2023 IEEE International Conference on Soft Robotics (RoboSoft)*. IEEE, 2023, pp. 1–8.

[26] R. M. Murray, Z. Li, and S. S. Sastry, *A mathematical introduction to robotic manipulation*. CRC press, 2017.

[27] F. Renda, C. Armanini, A. Mathew, and F. Boyer, "Geometrically-exact inverse kinematic control of soft manipulators with general threadlike actuators' routing," *IEEE Robotics and Automation Letters*, vol. 7, no. 3, pp. 7311–7318, 2022.